The following publication Wong, W. C., Ng, S. M., Wong, H. F., Mak, C. L., & Leung, C. W. (2017). Spin-valve junction with transfer-free MoS 2 spacer prepared by sputtering. IEEE Transactions on Magnetics, 53(11), 1600205, 1-5 is available at https://doi.org/10.1109/TMAG.2017.2733004.

Spin-Valve Junction with Transfer-Free MoS_2 Spacer Prepared by Sputtering

W.C. Wong, S.M Ng, H.F Wong, C.L. Mak and C.W. Leung*

Department of Applied Physics, The Hong Kong Polytechnic University, Hung Hom, Kowloon, Hong Kong

The prospects of spintronic devices based on two-dimensional (2D) materials originate from their outstanding spin-related properties. Fabrication of such devices typically involves transfer processes that yield inferior interfaces due to trapped contaminants or cavities at 2D material/electrode interfaces. Here we report a transfer-free fabrication process of MoS_2 films by RF magnetron sputtering, and demonstrate its application in the LSMO/MoS_2/NiFe spin valve structure. Raman spectroscopy shows E_{2g} and A_{1g} vibration modes of MoS_2, suggesting the growth of crystalline MoS_2 layers. A giant magnetoresistance ratio of 0.8% at 20 K was observed. The results suggest a scalable route for fabricating MoS_2-based electronic and spintronic devices with a transfer-free process for obtaining reliable contacts.

***Index Terms*—device fabrication; MoS_2; spin valve; transfer-free.**

I. Introduction

Spintronics is widely applied in hard disk read heads and non-volatile magnetoresistive random-access memories (MRAM), as well as magnetic sensors with ultra-high sensitivities. Simple spintronic devices are based on giant magnetoresistance (GMR) or tunneling magnetoresistance (TMR) with spin valve structure.[1] The performance of such devices depends highly on the spin retention capability of the spacer material. Recent researches have identified candidate materials such as highly-doped Si [2, 3], GaAs [4] and graphene [5-7], with the potential as channel materials for spin logic devices.[8]

Two-dimensional materials such as graphene or MoS_2 possess behaviour that are well-suited for electronic device. For example, the high on-off ratios of two-dimensional material-based transistors have drawn much attention for replacement of silicon transistors. Graphene also shows outstanding spin-related behavior. Due to the low atomic mass of carbon atoms, graphene shows long spin diffusion length (3-12 μm at 300 K) as compared with other materials (1 μm for Cu [9] or 0.6 μm for Al [10] at 4.2 K).

Compared with graphene, MoS_2 is more often used in optoelectronic applications [11-13]. However, MoS_2 also have some special spin-related properties. Spin lifetime in the order of nanoseconds was recorded in MoS_2, where the crystal symmetry can be easily broken by substrate effect or rippling; if the symmetry is retained a strong spin-retaining ability is anticipated.[14]

A number of attempts were made to study MoS_2-based spintronic devices. Fe/MoS_2/Fe junctions were predicted to yield a large magnetoresistance (MR) of 300% by fully atomistic first-principle transport calculation, due to the strong hybridization between Fe and S atoms which induces efficient spin injection.[15] On the other hand, in-plane (edge contacted) Fe/MoS_2/Fe junctions are estimated to give 150% magnetoresistance using non-equilibrium Green's function.

Corresponding author: C.W. Leung (e-mail: dennis.leung@polyu.edu.hk).

Color versions of one or more of the figures in this paper are available online at http://ieeexplore.ieee.org.

Digital Object Identifier (inserted by IEEE).

Experimentally, NiFe/MoS_2/NiFe junction showed 0.73% MR ratio, which is far worse than the calculation results.[16] Attempts of preparing the spacer with direct chemical vapour deposition rather than wet transfer process has led to significant improvement of MR in boron nitride-based magnetic tunnel junctions.[17-19] Apart from the elimination of surface contaminants or cavities at the electrode surfaces during the wet transfer process, suppression of electrode surface oxidation was suggested as a main contribution to the improved MR performance.[20] For scalable production of MoS_2, however, physical vapour deposition is the method of choice due to the capability of preparing ultrathin films with high uniformity over extended regions.[21] Preparation of high-quality MoS_2 films by pulsed laser deposition (PLD)[22, 23] and sputtering [24] have been reported.

In this report, we fabricate $La_{0.7}Sr_{0.3}MnO_3$ (LSMO)/MoS_2/$Ni_{0.8}Fe_{0.2}$ (NiFe) spin valve devices, with the MoS_2 spacer layer prepared by RF magnetron sputtering. LSMO bottom electrode is used for its chemical stability. We demonstrate the capability of preparing simple spintronic structure incorporated with two-dimensional materials, and highlights the prospect of scalable device applications.

II. Experimental Procedure

LSMO (20 nm)/MoS_2 (2 nm)/NiFe (5 nm) spin valve structure, in the current-perpendicular-to-plane (CPP) geometry, was investigated in this work (Fig. 1(a)). LSMO was deposited on $SrTiO_3$ (STO) substrates. For high-quality LSMO growth, buffered-HF treatment was performed on the substrates before film growth to obtain atomically flat, Ti-surface-terminated surfaces.[25] LSMO was deposited by PLD under an oxygen ambient of 120 mTorr at 700°C, in a chamber with a base pressure better than 6 μTorr. A KrF laser (248 nm) was used, with the laser energy of 220 mJ and a repetition rate of 5 Hz. The deposited films were post-annealed *in situ* at 650°C under 10 Torr of oxygen ambient.

Subsequently, RF magnetron sputtering was used to prepare the spacer layer from a MoS_2 target at room temperature, with an Ar pressure of 6 mTorr using 50 W RF power. To improve

the crystallinity of the deposited MoS_2, the samples were annealed *ex situ* at 450°C in nitrogen at atmosphere pressure. Finally, e-beam evaporation was used to deposit the top NiFe electrode and a gold capping layer (50 nm). For preparing devices suitable for CPP-type measurements, crossbar four-point measurement patterns with junction area (100×100) μm^2 were prepared, by using shadow mask for defining the electrodes of various layers (Fig. 1(b)).

The deposited films were characterized by Raman spectroscopy (HORIBA HR800) to inspect the quality of the MoS_2 spacer. Microstructural analysis of the samples were performed by atomic force microscopy (AFM, Burker Nanoscope 8) and x-ray diffractometry (Rigaku Smartlab). Magnetic hysteresis loops were obtained by vibrating sample magnetometer (Quantum Design model 6000.)

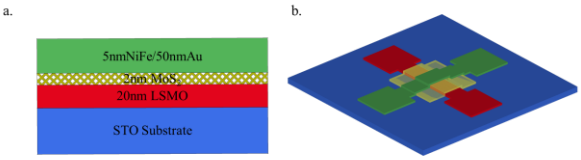

Fig.1 Schematic illustration of the device structure. (a) Cross-sectional view of multilayers; (b) three-dimensional illustration of CPP device structure.

III. RESULTS AND DISCUSSION

Fig. 2 shows the characterization of the STO substrate and the LSMO layer. After buffered HF treatment, the AFM image of the STO substrate (inset of Fig. 2(a)) shows a terraced pattern. This result suggests that flat STO substrates were produced. Subsequently LSMO was deposited on the flat STO substrate. XRD θ-2θ scan (Fig. 2(a)) indicates only STO (002) and LSMO (002) peaks were obtained, and together with the narrow LSMO (002) peak of full-width-at-half-maximum (FWHM) ~ 0.35°, we conclude that epitaxial LSMO films were grown on STO substrates.

Temperature-dependent resistance measurement (Fig. 2(b)) was performed on the LSMO film between 20 and 320 K. The result shows a positive slope over the whole temperature range measured. Typically, the Curie temperature (T_C) of LSMO films can be determined from the peak of the resistance-temperature plot.[26] Such a peak is not observed in Fig. 2(b), which indicates the T_C is larger than 320 K (noting that bulk LSMO has T_C ~ 370 K). All results in Fig. 2 confirm the good-quality of LSMO films deposited in this work.

For meaningful comparison of our results with those in literature, it is important to produce MoS_2 spacers with reasonable quality. Raman spectroscopy is an established method for characterizing 2D materials, and for MoS_2 Raman spectra the E_{2g} and A_{1g} peaks are strongly dependent on the number of atomic layers.[27] Three samples of MoS_2 deposited on Si were investigated, the conditions of which are summarized in Table I, and the Raman spectra of the samples are shown in Fig. 3. Both high and low temperature deposition of MoS_2 have been reported to produce MoS_2 films. [22, 28]To investigate the effect of deposition temperature on the quality of MoS_2 films, samples deposited at room temperature and 500°C were compared (Table I).

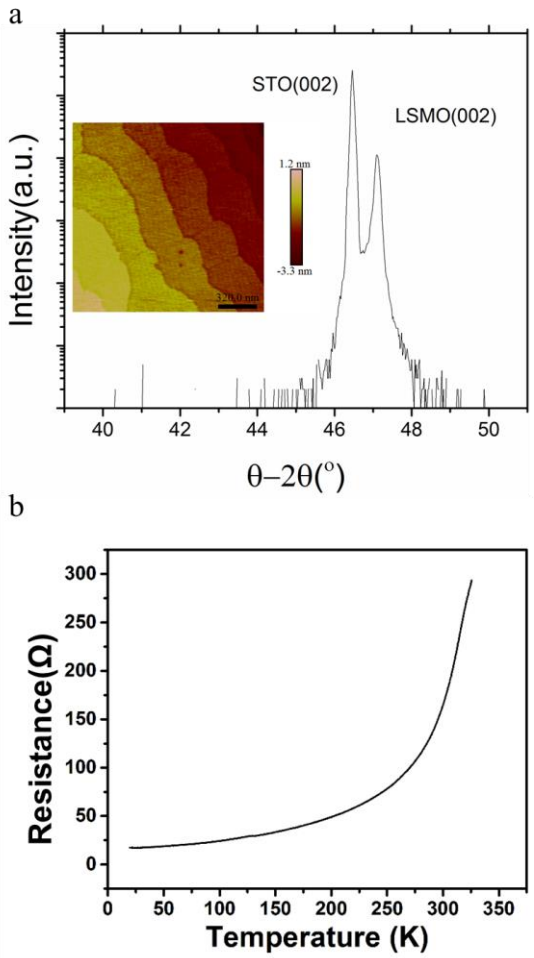

Fig. 2 Characterization of 20-nm LSMO film on STO (001) substrate. (a) θ-2θ scan. Inset: AFM micrograph of the STO substrate after buffered-HF treatment. (b) Temperature-dependent resistance measurement.

TABLE I
DEPOSITION CONDITIONS FOR MoS_2 ON Si FOR OPTIMIZATION PURPOSE.

Sample	Deposition Temperature	Thickness
A	Room temperature	20 nm
B	Room temperature	10 nm
C	500°C	20 nm

As shown in Fig. 3(a), the Raman spectra of all samples show peaks at 385, 408 and 520 cm^{-1}; these peaks are assigned as the E_{2g} and A_{1g} peaks of MoS_2, and the Si substrate peak, respectively. The results indicate that MoS_2 was successfully deposited on Si. The FWHM of A_{1g} peak for Sample C is 16 cm^{-1}, and 9 cm^{-1} for room temperature-deposited samples, despite all samples have undergone post-annealing. The

intensities of Samples A and B are also high than Sample C, even Sample B is thinner than Sample C. The large FWHM of Sample C indicates an inferior crystallinity. This arises from the low vapour pressure of the sulphur that leads to its excessive loss during high temperature deposition, which yields a high concentration of sulphur vacancies.[22, 29] Room temperature deposition of MoS_2, followed by post-annealing, demonstrates better film crystallinity.

The significance of post-annealing is highlighted in Fig. 3(b), which shows the Raman spectra of Sample B before (black) and after (red) post-annealing at 450°C in nitrogen at atmospheric pressure. The FWHM of A_{1g} peak before and after post-annealing are 11 and 9 cm^{-1}. Moreover, the peak intensity is increased after post-annealing, which can be attributed to the improved crystallinity of the MoS_2 by post-annealing as room temperature deposition is known to produces amorphous MoS_2.[28] On the other hand, post-annealing has no impact on high temperature-grown MoS_2, as evidenced from the lack of difference in the Raman spectra profile for Sample C before and after post-annealing (Fig. 3(c)). As much thinner MoS2 layer is needed for spacer layer in spin valves, the effect of post-annealing on 2 nm MoS_2 deposited on Si was also studied (Fig. 4(a)). As in the case of Sample B (Fig. 3(b)), signature Raman peaks of MoS_2 were retrieved after the post-annealing process for the 2 nm MoS_2 sample.

Using the optimized conditions for MoS_2 growth on Si substrates (room-temperature deposition followed by post-annealing in nitrogen), MoS_2 spacer was prepared on LSMO and the Raman spectrum of LSMO/MoS_2 (Fig. 4(b)) shows the signature E_{2g} and A_{1g} peaks. This result shows that crystalline MoS_2 was deposited on STO/LSMO. The deposited MoS2 on LSMO shows a high level of smoothness (Fig. 4(c), root-mean-squared roughness = 0.31 nm). Given the lack of lattice matching conditions between MoS_2 and the receiving surfaces tested (Si and LSMO), we speculate the method can be adapted on different substrates for fabricating various MoS_2-based devices. [22, 24]

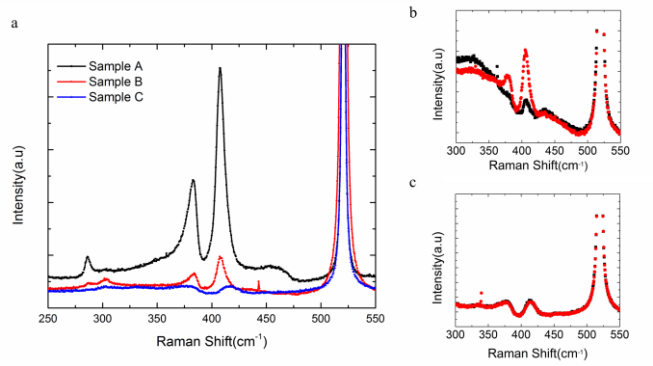

Fig.3 Raman spectra of sputtered MoS_2 films with different deposition and annealing conditions. (a) All the three samples in Table I after post-annealing. (b) Sample B before (black) and after (red) post-annealing. (c) Sample C before (black) and after (red) post-annealing.

The NiFe/Au top electrode was finally deposited on top of MoS_2 by e-beam evaporation; evaporation method was adopted as it prevents the damage of MoS_2 by energetic species bombardment in deposition techniques like sputtering or PLD. This is partly justified by magnetic measurement of the spin valve multilayer stacks: the presence of a double coercivity behavior in spin valves with ultrathin MoS_2 (Fig. 5) asserts the smoothness of the layer that is reasonably free from pinholes.[30] The magnetic hysteresis loop show double coercivity at 18 Oe and 33 Oe at 20 K, which correspond to the coercivities of LSMO and NiFe, respectively. The double coercivity suggests the MoS_2 spacer magnetically decouples the LSMO and NiFe layers.

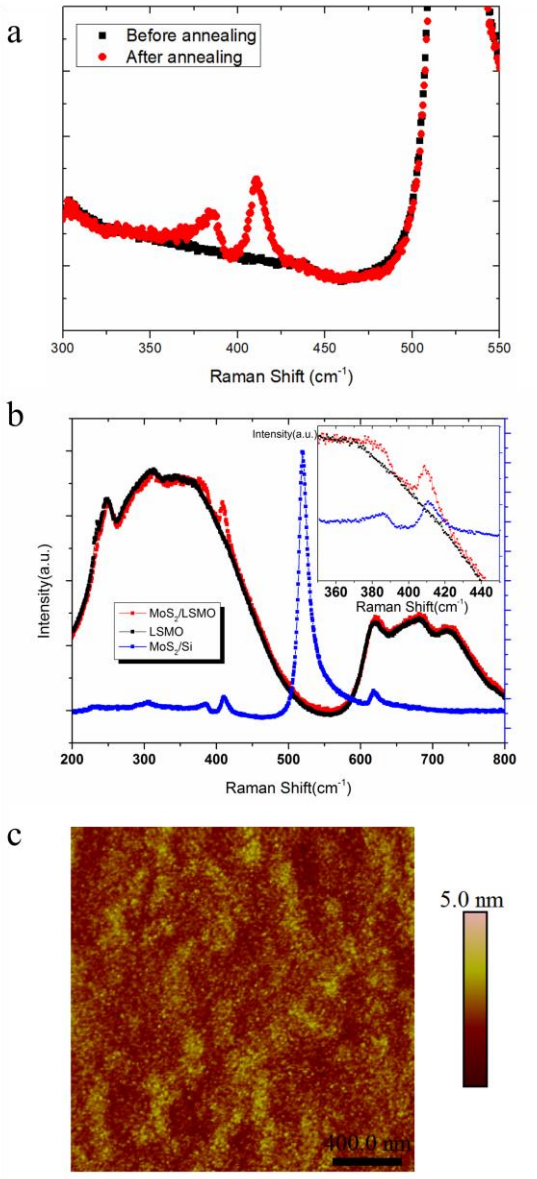

Fig. 4 (a) Raman spectra of 2 nm MoS_2 on Si before (black) and after post-annealing (b) Raman spectra of 2 nm MoS_2 on STO/LSMO (red) and Si (blue). Black trace shows the spectrum of STO/LSMO. The board peak from 200 to ~ 450 cm^{-1} is the peak of STO substrate. Inset highlights the data between 350 and 450 cm^{-1}. (c) AFM micrograph of the LSMO/MoS_2 after post-annealing process.

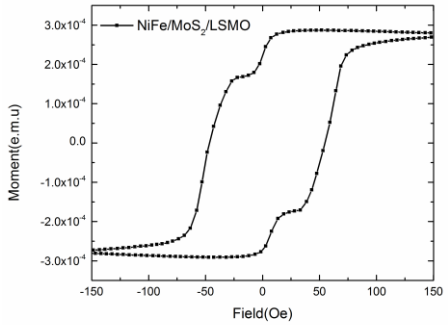

Fig. 5 Hysteresis loop of LSMO/MoS_2/NiFe junction at 20 K

Magnetoresistance (MR) measurement of the STO/LSMO (20 nm)/MoS_2 (2 nm)/NiFe (5 nm)/Au (50 nm) spin valve device was performed at 20 K. At this temperature, the zero-field resistance of the device was around 330 Ω by four-point measurement. The MR result is shown in Fig. 6. A negative MR signal is obtained, which is similar to the result of LSMO/$BaTiO_3$(BTO)/NiFe with no polarization of BTO.[31] The MR ratio is obtained by following equation :

$$MR\ ratio\ (\%) = \frac{R_{anti-paraellel} - R_{paraellel}}{R_{paraellel}} \times 100\%$$

The MR ratio of the device at 20 K is 0.8%. The switching field in MR curve matches with the double coercivity from hysteresis loop in Fig. 5, which indicates the MR signal is due to the spin valve junction. To rule out the possibility of anisotropic magnetoresistance (AMR) from the magnetic electrodes, measurement was repeated by rotating the in-plane magnetic field through 90° (inset of Fig. 6) and identical negative MR behavior was measured. The result confirms that the MR obtained was due to the spin valve effect of the device.

The MR ratio of our MoS_2-based spin valve junction is comparable with previous experiment on transferred MoS_2 spin valves [16]. One should note, however, that our MoS_2 layer was polycrystalline while that in Ref. 16 was (almost) single-crystalline, which is expected to yield better MR behavior. The wet transfer method, however, may trap contaminants which adversely affect the contact interfaces. In addition, the preparation of CPP device structure involves transfer of MoS_2 onto the junction sites, which is difficult to be achieved by wet transfer method but is virtually effortless by physical vapour deposition of the spacer layer.

Physical vapour deposition (and magnetron sputtering in particular) can produce ultrathin films of uniform thickness over large areas (typically above 1 cm), and can be readily adaptable for scaled-up preparation of MoS_2 devices. With the careful control of deposition parameters ultrathin films (down to monolayer thickness) can be achieved.[21] The deposition of MoS_2 spacer, as demonstrated in this work, provides the prospect of repeatable preparation of large-size MoS_2 that is contaminants-free process for device fabrication.

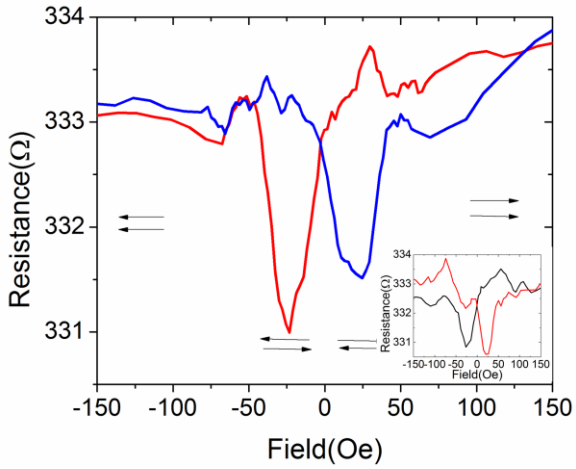

Fig.6 MR behaviour of LSMO/MoS_2/NiFe spin valve device. Inset: MR plot of the same device with applied magnetic field rotated 90° in the substrate plane. All measurements were done at 20 K.

IV. CONCLUSIONS

In conclusion, LSMO/MoS_2/NiFe spin valve junction was fabricated, with the MoS_2 spacer deposited by RF sputtering deposition at room temperature and annealed subsequently. The MoS_2 layer was effective in decoupling the two magnetic electrodes and the spin valve multilayer showed double coercivity behavior. A magnetoresistance ratio of 0.8% at 20 K was demonstrated. This work demonstrated an alternative method to produces MoS_2 electronic and spintronic devices without undergoing transfer process that may lead to extensive interfacial contaminations and irreproducible device performances.

ACKNOWLEDGMENT

The work is supported by PolyU (G-YBJ1, G-YBPU, 1-BBAD, 1-ZE25) and University Grants Council of HKSAR (PolyU 153015/14P).

REFERENCES

[1] J. Sinova and I. Zutic, "New moves of the spintronics tango," *Nat Mater*, 10.1038/nmat3304 vol. 11, no. 5, pp. 368-71, Apr 23 2012.

[2] S. Toshio, S. Tomoyuki, O. Tohru, S. Masashi, S. Yoshishige, and N. Kiyoshi, "Room-Temperature Electron Spin Transport in a Highly Doped Si Channel," *Applied Physics Express*, vol. 4, no. 2, p. 023003, 2011.

[3] I. Appelbaum, B. Huang, and D. J. Monsma, "Electronic measurement and control of spin transport in silicon," *Nature*, 10.1038/nature05803 vol. 447, no. 7142, pp. 295-8, May 17 2007.

[4] B. Q. Huang and I. Appelbaum, "Spin dephasing in drift-dominated semiconductor spintronics devices," (in English), *Physical Review B*, vol. 77, no. 16, p. 165331, Apr 2008.

[5] P. J. Zomer, M. H. D. Guimaraes, N. Tombros, and B. J. van Wees, "Long-distance spin transport in high-mobility graphene on hexagonal boron nitride," (in English), *Physical Review B*, vol. 86, no. 16, p. 161416, Oct 31 2012.

[6] T. Y. Yang *et al.*, "Observation of long spin-relaxation times in bilayer graphene at room temperature," (in English), *Phys Rev Lett*, vol. 107, no. 4, p. 047206, Jul 22 2011.

[7] W. Han *et al.*, "Tunneling spin injection into single layer graphene," (in English), *Phys Rev Lett*, vol. 105, no. 16, p. 167202, Oct 15 2010.

[8] W. Han, R. K. Kawakami, M. Gmitra, and J. Fabian, "Graphene spintronics," *Nat Nanotechnol*, Review vol. 9, no. 10, pp. 794-807, Oct 2014.

[9] F. J. Jedema, A. T. Filip, and B. J. van Wees, "Electrical spin injection and accumulation at room temperature in an all-metal mesoscopic spin valve," (in English), *Nature*, 10.1038/35066533 vol. 410, no. 6826, pp. 345-348, Mar 15 2001.

[10] F. J. Jedema, H. B. Heersche, A. T. Filip, J. J. Baselmans, and B. J. van Wees, "Electrical detection of spin precession in a metallic mesoscopic spin valve," *Nature*, 10.1038/416713a vol. 416, no. 6882, pp. 713-6, Apr 18 2002.

[11] Z. Yin *et al.*, "Single-layer MoS2 phototransistors," *ACS Nano*, vol. 6, no. 1, pp. 74-80, Jan 24 2012.

[12] O. Lopez-Sanchez, D. Lembke, M. Kayci, A. Radenovic, and A. Kis, "Ultrasensitive photodetectors based on monolayer MoS2," *Nat Nanotechnol*, Letter vol. 8, no. 7, pp. 497-501, Jul 2013.

[13] P.-L. Néstor *et al.*, "CVD-grown monolayered MoS 2 as an effective photosensor operating at low-voltage," *2D Materials*, vol. 1, no. 1, p. 011004, 2014.

[14] H. Ochoa and R. Roldán, "Spin-orbit-mediated spin relaxation in monolayer MoS_2," *Physical Review B*, vol. 87, no. 24, p. 245421, 06/17/ 2013.

[15] K. Dolui, A. Narayan, I. Rungger, and S. Sanvito, "Efficient spin injection and giant magnetoresistance in Fe/MoS_2/Fe junctions," *Physical Review B*, vol. 90, no. 4, p. 041401, 07/02/ 2014.

[16] W. Wang *et al.*, "Spin-Valve Effect in NiFe/MoS2/NiFe Junctions," *Nano Lett*, vol. 15, no. 8, pp. 5261-7, Aug 12 2015.

[17] A. Dankert, M. V. Kamalakar, A. Wajid, R. S. Patel, and S. P. Dash, "Tunnel magnetoresistance with atomically thin two-dimensional hexagonal boron nitride barriers," (in English), *Nano Research*, vol. 8, no. 4, pp. 1357-1364, Apr 2015.

[18] M. Piquemal-Banci *et al.*, "Magnetic tunnel junctions with monolayer hexagonal boron nitride tunnel barriers," (in English), *Applied Physics Letters*, vol. 108, no. 10, p. 102404, Mar 7 2016.

[19] P.-B. Maëlis *et al.*, "2D-MTJs: introducing 2D materials in magnetic tunnel junctions," *Journal of Physics D: Applied Physics*, vol. 50, no. 20, p. 203002, 2017.

[20] Z. Simon, M. Péter, A. F. V. Carlos, and S. Christian, "Role of hexagonal boron nitride in protecting ferromagnetic nanostructures from oxidation," *2D Materials*, vol. 3, no. 1, p. 011008, 2016.

[21] J. Tao *et al.*, "Growth of wafer-scale MoS2 monolayer by magnetron sputtering," *Nanoscale*, 10.1039/C4NR06411A vol. 7, no. 6, pp. 2497-2503, 2015.

[22] M. I. Serna *et al.*, "Large-Area Deposition of MoS2 by Pulsed Laser Deposition with In Situ Thickness Control," *ACS Nano*, vol. 10, no. 6, pp. 6054-61, Jun 28 2016.

[23] W. Jie, Z. Yang, F. Zhang, G. Bai, C. W. Leung, and J. Hao, "Observation of Room-Temperature Magnetoresistance in Monolayer MoS2 by Ferromagnetic Gating," *ACS Nano*, vol. 11, no. 7, pp. 6950-6958, 2017/07/25 2017.

[24] J. Tao *et al.*, "Growth of wafer-scale MoS2 monolayer by magnetron sputtering," *Nanoscale*, 10.1039/C4NR06411A vol. 7, no. 6, pp. 2497-503, Feb 14 2015.

[25] M. Kawasaki *et al.*, "Atomic Control of the $SrTiO_3$ Crystal Surface," *Science*, vol. 266, no. 5190, pp. 1540-2, Dec 02 1994.

[26] J. R. Sun, H. W. Yeung, H. K. Wong, T. Zhu, and B. G. Shen, "Effects of vacuum annealing on the transport property of La0.67Sr 0.33MnO3-δ films," *Eur. Phys. J. B*, vol. 35, no. 4, pp. 481-491, 2003.

[27] H. Li *et al.*, "From Bulk to Monolayer MoS2: Evolution of Raman Scattering," (in English), *Advanced Functional Materials*, vol. 22, no. 7, pp. 1385-1390, Apr 10 2012.

[28] M. E. McConney *et al.*, "Direct synthesis of ultra-thin large area transition metal dichalcogenides and their heterostructures on stretchable polymer surfaces," *Journal of Materials Research*, vol. 31, no. 07, pp. 967-974, 2016/004/14 2016.

[29] M. S. Donley, P. T. Murray, S. A. Barber, and T. W. Haas, "Deposition and Properties of Mos2 Thin-Films Grown by Pulsed Laser Evaporation," (in English), *Surface & Coatings Technology*, vol. 36, no. 1-2, pp. 329-340, Dec 1 1988.

[30] C. W. Leung, M. E. Vickers, J. D. R. Buchanan, and M. G. Blamire, "A study of conventional top spin valve structure through the built-up samples technique," (in English), *Journal of Magnetism and Magnetic Materials*, vol. 269, no. 1, pp. 15-29, Feb 2004.

[31] H. M. Yau *et al.*, "Low-field Switching Four-state Nonvolatile Memory Based on Multiferroic Tunnel Junctions," *Sci Rep*, Article vol. 5, p. 12826, Aug 04 2015.